ELSEVIER

Ceramics International 27 (2001) 373–384

CERAMICS INTERNATIONAL

www.elsevier.com/locate/ceramint

PZT/PLZT ceramics prepared by hydrolysis and condensation of acetate precursors

Wein-Duo Yang *

Department of Chemical Engineering, National Kaohsiung University of Applied Sciences, Kaohsiung 80807, Taiwan

Received 3 January 2000; received in revised form 8 September 2000; accepted 8 September 2000

Abstract

Titanyl zirconyl acetate was prepared by chelating titanium isopropoxide with acetic acid, and was used as a precursor in a sol-gel process to obtain PZT and PLZT powders. The combined results of the DTA/TGA, FTIR and SEM studies indicate that the PLZT-precursor contained a higher mol fraction of acetate groups and that polycondensation was slower, resulting in a small particle size for the PLZT powder. X-ray photoelectron spectroscopy (XPS) was used to detect Ti oxidation states on the surface of the PZT and PLZT bulk ceramics sintered at various temperatures. The Ti binding energy of the PLZT powders prepared at various temperatures were all lower than those of the corresponding PZT powders, indicating a relatively higher Ti^{3+} concentration on the PLZT surface. This higher Ti^{3+} surface concentration is responsible for the higher relative dielectric constant measured for the PLZT bulk ceramics.

Keywords: B. X-ray methods; D. PZT; D. PLZT; Titanyl zirconyl acetate

1. Introduction

The crystal lattice of lead zirconate titanate ($Pb(Zr_{1-x}, Ti_x)O_3$, PZT) is similar to that of $BaTiO_3$; both crystallize in a perovskite structure. PZT has, compared with $BaTiO_3$, a more versatile range of applications due to its higher application temperature and stronger piezoelectric properties [1–3]. Depending on the temperature and the amount of $PbZrO_3$ in PZT several crystal phases are observed. The compound crystallizes in a tetragonal phase (high $PbTiO_3$ content) or a rhombohedral phase. At room temperature and a high $PbZrO_3$ content ($>92\%$), an orthorhombic phase is observed. At higher temperatures, the phases convert to a cubic structure (the actual temperature being dependent on the composition) [4]. In engineering applications, a compound with the formula $Pb(Zr_{0.54},Ti_{0.46})O_3$ is widely used [3]. This composition lies near a morphotropic phase boundary of the phase diagram; i.e. at room temperature, both the rhombohedral and tetragonal phase coexist in this composition. This fact greatly increases the material's piezoelectric properties.

Other oxides can be added to improve PZT's properties [5–8]. Substituting the A-sites of Pb^{2+} with La^{3+} or Nd^{3+}, or substituting the B-sites of Zr^{4+} and Ti^{4+} with Nb^{5+} or Ta^{5+}, leads to a considerable improvement in the electric properties of PZT. As the electric valence of the added cations is larger than the electric valence of the original cations, the crystal cell, for reasons of electric neutrality, contains a vacancy in the A-site (Pb^{2+}) or B site (Zr^{4+} or Ti^{4+}), respectively. As an average, the substitution of two A-site Pb^{2+} ions with two aliovalent La^{3+} ions will result in one vacancy of an A-site in the crystal lattice. The same holds true for a B-site substitution of Zr^{4+} or Ti^{4+} with aliovalent Nb^{5+} or Ta^{5+}. It is a commonly accepted fact that this substitution and the resulting vacancies in the crystal lattice considerably change the material properties, such as dielectric constant, dielectric loss, elastic modulus, etc.

Recently, an organic technique — the so-called sol-gel process which uses metal alkoxides as a starting material — has been used in preparing powders of homogeneous compositions. Stoichiometric ultrafine powders have been obtained [9–10]. Metal alkoxides react readily with moisture, but by doing so form a hydrous gel with a reduced solubility in the solvent, making them unusable in the process. Some sol–gel processes use acetic

* Fax: +886-7-3830674.
E-mail address: ywd@cc.kuas.edu.tw

0272-8842/01/$ - see front matter
PII: S0272-8842(00)00091-2

acid as a chelating ligand for the metal alkoxide, creating a metal acetate precursor. This precursor is not moisture sensitive and can be produced cheaply, making it convenient for use in the process [11–12]. The acetate precursor used in the present study was soluble in water and didn't lead to the formation of hydrous titania [13]. The sol-gel process has a promising potential for further development. In recent years, a number of studies in which acetic acid has been used as a chelating agent for the metal alkoxide has been reported [14–17].

In this study, a mixed titanyl zirconyl acetate precursor gel was prepared in an acidic solution by chelating a mixture of titanium and zirconium alkoxides with acetic acid. The gel was then dried and calcined to yield the PZT powder. Separately, a lead lanthanum zirconate titanate ($(Pb_{1-x}, La_x)(Zr_{1-y}, Ti_y)O_3$, PLZT) powder was prepared using a similar procedure. Combining results from DTA/TGA, FTIR and XRD studies, the formation mechanisms of the powders were investigated. Furthermore, XPS was used to characterize Ti oxidation states on the surface of the PZT and PLZT powders and to establish a relationship between low valence Ti (Ti^{3+}) and the electric properties of the material.

2. Experimental

2.1. Preparation of PZT/PLZT

Zirconium n-propoxide and titanium isopropoxide were mixed in a molar ratio of 54: 46. The alkoxide mixture was brought to reaction with excess acetic acid (molar ratio HOAc/(Ti + Zr) = 10) to obtain a mixed titanyl zirconyl acetate precursor ($Ti(Zr)(OAc)_x(OR)_y$). Degassed water was added into the vigorously stirred mixture, causing the hydrolysis (fast) of the titanyl zirconyl acetate. A clear solution of $Ti(Zr)(OAc)_x(OH)_y$ was obtained [12]. All steps were carried out at room temperature.

A solution of lead acetate (and in the preparation of PLZT also lanthanum acetate) in acetic acid was added slowly to the previously prepared titanyl zirconyl acetate precursor while stirring the mixture held in a bath at 60°C. After mixing, hydrolysis (fast) and polycondensation (slow) took place resulting in the formation of a clear sol.

The clear sol, cast into dishes, usually gelated through the polycondensation process; a semitransparent gel with a crosslinked network structure was obtained within 1–3 h. The reactions are summorized below:

$$x\ \mathrm{HOAc} + \mathrm{Ti(OR)_4} + \mathrm{Zr(OR)_4} \rightarrow \mathrm{Ti(Zr)Ac}_x\mathrm{(OR)}_{8-x}$$

$$\mathrm{Ti(Zr)Ac}_x\mathrm{(OR)}_{8-x} + \mathrm{H_2O} \xrightarrow{\text{hydrolysis}} \mathrm{Ti(Zr)Ac}_x\mathrm{(OH)}_{8-x}$$

$$\mathrm{Ti(Zr)Ac}_x\mathrm{(OH)}_{8-x} \xrightarrow{\text{polycondensation}} \text{gel}$$

All of the gels obtained in this manner (except the ones used for laser particle size distribution analysis) were freeze-dried and then crushed in a ball mill (ZrO_2 ball, 200–250 rpm, for 24 h) into very fine white gel powders. The cation ratio was Pb: Zr: Ti = 1: 0.54: 0.46, and Pb: La: Zr: Ti = 0.91: 0.09: 0.54: 0.46 (given by the ratio of chemicals mixed) to obtain $Pb(Zr_{0.54},Ti_{0.46})O_3$ and $(Pb_{0.91},La_{0.09})(Zr_{0.54},Ti_{0.46})O_3$, respectively. The flow chart of the sol-gel preparation of the PZT and PLZT powders is shown in Fig. 1.

The dried gels were calcined at 300–700°C for 3–8 h In this manner, highly crystalline (see XRD and FTIR results below) PZT and PLZT powders were prepared (PZT: yellow, PLZT: orange color). The calcined PZT and PLZT powders were compacted at 110 MPa in a stainless steel die of 13 mm in diameter. The green bodies were sintered at temperatures between 1100 and 1350°C for 2 h in an electric furnace. Due to the fact that considerable amounts of PbO evaporate at temperatures above 888°C, a sintering method similar to the one applied by Snow [18], which compensates for the PbO loss, had to be applied. The green bodies were sintered on a ZrO_2 plate covered by an aluminum oxide crucible, under an atmosphere containing PbO. The partial pressure of PbO was generated by a solid mixture of 90% $PbZrO_3$ and 10 wt.% PbO.

2.2. Testing methods

Differential thermal analysis (DTA) and thermogravimetric analysis (TGA) were used to characterize

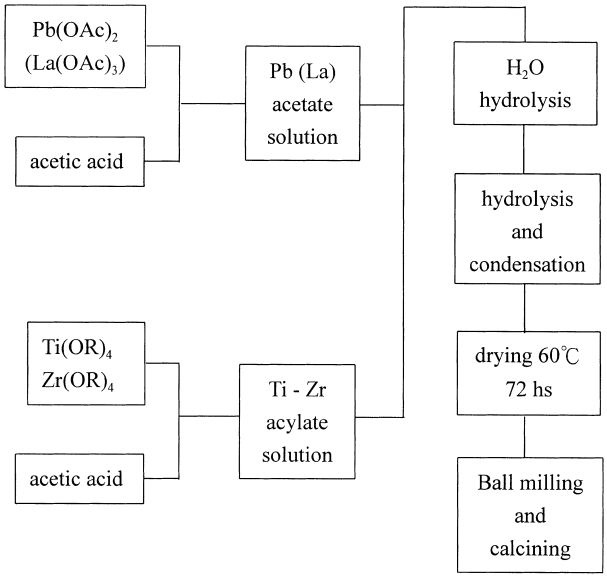

Fig. 1. Preparation route for the PZT and PLZT powders via a sol-gel process.

the precursors. A heating rate of 10°C min^{-1} and a N_2 atmosphere, were used in both techniques. Fourier transfer infrared spectroscopy (FTIR) and X-ray diffraction (XRD) analysis were used to analyze the precursors calcined at various temperatures. The particle size of the powders was measured by scanning electron micrography (SEM) after freeze-drying, and their homogeneity was determined with a laser particle size distribution analyzer. After calcining and ball milling, the powders were screened (< 53 μm) and then pressed at 110 MPa in a stainless steel die to form green bodies having a diameter of 13 mm and a thickness of 3–4 mm. Dilatometry was used to study the sinterability of the green bodies. Dilatometric measurements were made using a heating rate of 10°C min^{-1} and a N_2 atmosphere.

Surface analysis of the PZT and PLZT samples were carried out using a V.G. Instruments X-ray photoelectron spectrometer. Mg K_α radiation was used as the X-ray source and the photoelectron peaks from the samples were numerically fitted using Lorentzian curves with an integral background subtraction and analyzed at an angle of 45° to the surface. The adventitious C 1s signal at 284.6 eV was used to calibrate the charge-shifted energy scale. The X-ray spot size was 600 mm and the resolution was about 0.8 eV always. The spectra represent original experimental data recorded to an accuracy of 0.2 eV. In addition, the spectra were deconvoluted for chemical identification using 100% Gaussian peaks.

The cross-sections of the sintered bodies were polished and etched in a concentrated HCl solution at 80–85°C for 1 h and then sputter-coated with Au. SEM was used to investigate the character of their surfaces. The sintered samples were polished into bodies of 2 mm in thickness and the surface coated with conductive silver paste as an electrode. After baking the electrodes at 700°C, the relative dielectric constants of the ceramic bodies were measured with an HP LCR analyzer 4284 A.

3. Results and discussion

3.1. Studies of precursor

3.1.1. Infrared spectrum analysis

The dried PZT/PLZT crystal powders calcined at various temperatures were characterized by FTIR (Fig. 2). There are two absorption bands in the vicinities of 1450 and 1560 cm^{-1} for the precursors dried at 100°C. These peaks are attributed to symmetric and asymmetric vibrations of the acetate group. When the difference between these two absorption peaks ($\triangle\nu$) is smaller than 80 cm^{-1}, acetate is typically a chelating bidentate ligand. When $\triangle\nu$ is larger than 160 cm^{-1}, the acetate group is typically a bridging bidentate ligand [19]. The value of $\triangle\nu$ was 145 cm^{-1} for the PZT [Fig. 2(A)], and 125 cm^{-1} for the PLZT precursor [Fig. 2(B)]. The difference of the PZT-precursor was larger than that of the PLZT precursor, meaning that the PZT-precursor contained more bridging bidentate ligands. More bridging bidentate ligands result in larger particles of the final powder (PZT), and more chelating bidentate ligands (PLZT) lead to a smaller particle size.

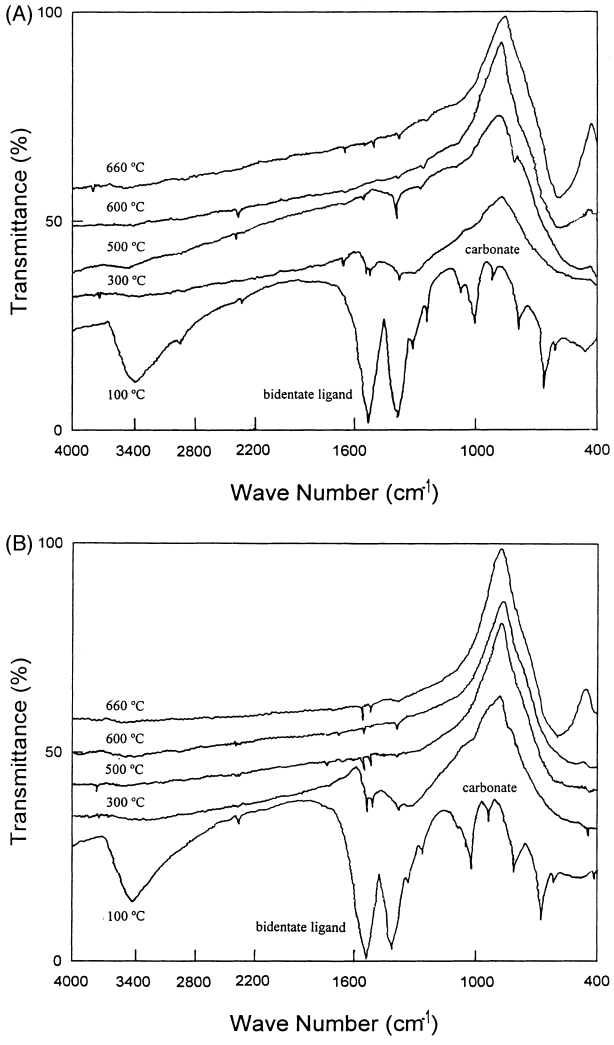

Fig. 2. FTIR spectra of the samples calcined at various temperatures for 4 h. (A) PZT precursor, (B) PLZT precursor.

The dried PZT-precursor gel calcined at 300°C shows absorption peaks near 860, 1100 and 1460 cm^{-1}. These peaks indicate the presence of carbonate in the dried gel [20]. The PZT-precursor gel calcined at 500°C shows a very weak absorption peak at 550 cm^{-1} which is characteristic for a perovskite phase [21]. This absorption peak becomes gradually stronger in the precursor gels calcined at 600 and 660°C, indicating that the formation of a perovskite phase starts to take place at about 500°C and increases in proportion with an increase in temperature.

The FTIR spectra of the PLZT-precursors calcined at various temperatures are shown in Fig. 2(B). These

spectra are similar to those of the PZT-precursors shown in Fig. 2(A). A detailed comparison reveals though that the absorption peak representing the perovskite structure is not significant at 600°C, indicating that the formation of a perovskite phase in PLZT takes place at a higher temperature.

3.1.2. DTA/TGA analyses

Fig. 3(A) (PZT) and (B) (PLZT) shows the DTA/TGA graphs of the precursor gels after drying. The DTA graph shows an endothermic peak in the vicinity of 100°C and the TGA graph indicates a relative weight loss. Both can be attributed to the evaporation of water from the precursor. A second endothermic peak at 280°C indicates the decomposition of the acetate groups to carbonate, a result in accordance with the FTIR spectra, which shows that at a temperature around 300°C the absorption peak of the acetate groups becomes weaker, indicating their decomposition.

The weight loss observed in the TGA analysis shows that the PZT-precursor contained 46 wt.% PZT, and the PLZT-precursor contained 37 wt.% PLZT. Therefore, the PLZT-precursor contained more organic species. The biggest portion of organic species should be acetate groups, because an additional amount of $La(OAc)_3$ was added during the preparation of the PLZT precursor. Perhaps the higher amount of acetate groups in the gel structure is responsible for an increased distance between the cations (Pb^{2+}, La^{3+}, Zr^{4+}, Ti^{4+} etc.) in the structure, which results in an inhibition of the formation of PLZT due to an increased reaction distance. This necessitates a higher reaction temperature for the formation of PLZT. Comparing the two DTA graphs for the PZT [Fig. 3(A)] and the PLZT [Fig. 3(B)] precursor, an exothermic peak of higher intensity is found for the PLZT precursor between 700 and 800°C. The corresponding DTA graph for the PLZT precursor does not show a weight loss between 700 and 800°C. The XRD pattern of the PLZT-precursor calcined at 700°C shows a small peak at $2\theta = 27.3°$, indicating that La_2O_3 existed in the microstructure [shown in Fig. 4(D)]. This peak indicates that during the formation process of PLZT, PZT is formed first as an intermediate step. The PZT then reacts further with the present La_2O_3 to form PLZT as the end product.

3.1.3. XRD analysis

The various dried gels calcined at different temperatures were characterized by XRD to identify their

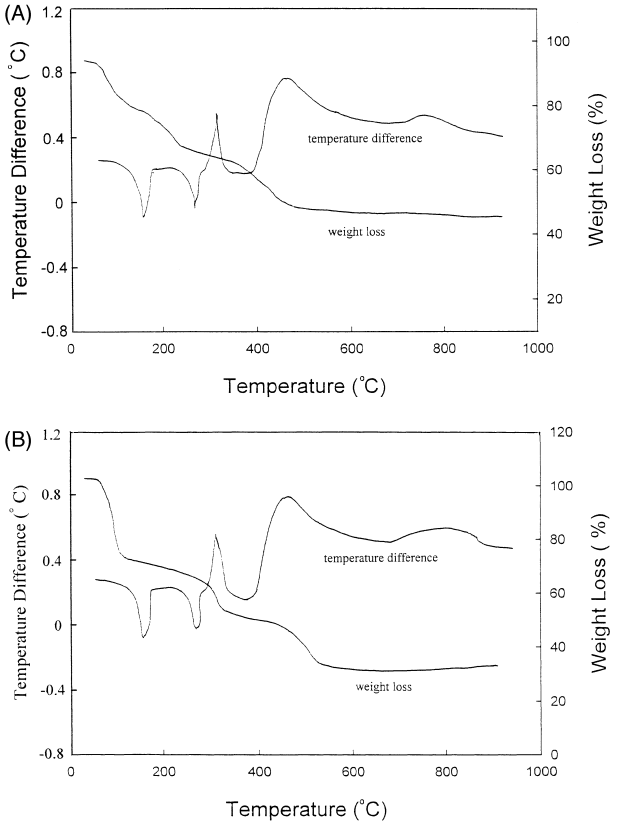

Fig. 3. The results of the DTA/TGA of the dried gels. (A) PZT precursor, (B) PLZT precursor.

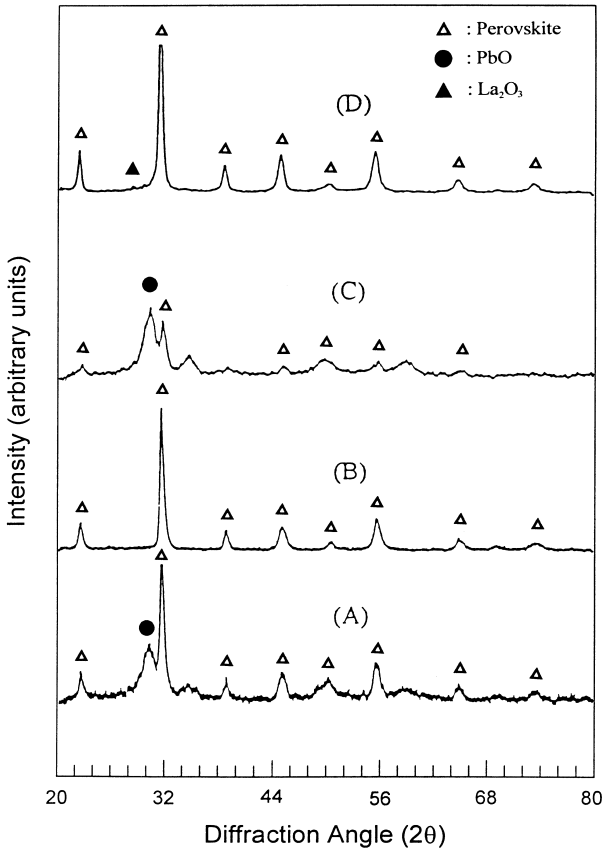

Fig. 4. The XRD patterns of the calcined powders. (A) PZT precursor calcined at 600°C; (B) PZT precursor calcined at 660°C; (C) PLZT precursor calcined at 600°C; (D) PLZT precursor calcined at 660°C.

respective crystal phases (Fig. 4). The figure shows that a perovskite phase had formed in the PZT-precursor calcined at 600°C [Fig. 4(A)], but a lot of PbO existed in the calcined powder as well. However, the PZT precursor calcined at 660°C did not contain any detectable amount of PbO and crystallized in a perfect perovskite structure [Fig. 4(B)].

In contrast, the PLZT precursor calcined at 600°C [Fig. 4(C)] shows a XRD pattern with fewer perovskite phases, but a significant amount of PbO in the gel. The PbO formed as a result of the decomposition of lead acetate via $PbCO_3$ and its following decarboxylation. The PLZT precursor calcined at 660°C [Fig. 4(D)] contained traces of La_2O_3 and perovskite phase (see DTA/TGA analysis). The results of the XRD study indicate similar formation temperatures for PZT (600°C) and PLZT (660°C) to those suggested by the FTIR study.

3.2. Powder properties

3.2.1. Homogeneity and powder particle size

The PZT and PLZT precursors calcined at 700°C for 8 h were characterized with a laser particle size distribution analyzer (Fig. 5). Comparing the particle size distribution of the two unmilled original calcined powders, the PZT powder, in which the precursor contained fewer acetate groups, was found to be less homogeneous. It also had larger aggregate particle sizes.

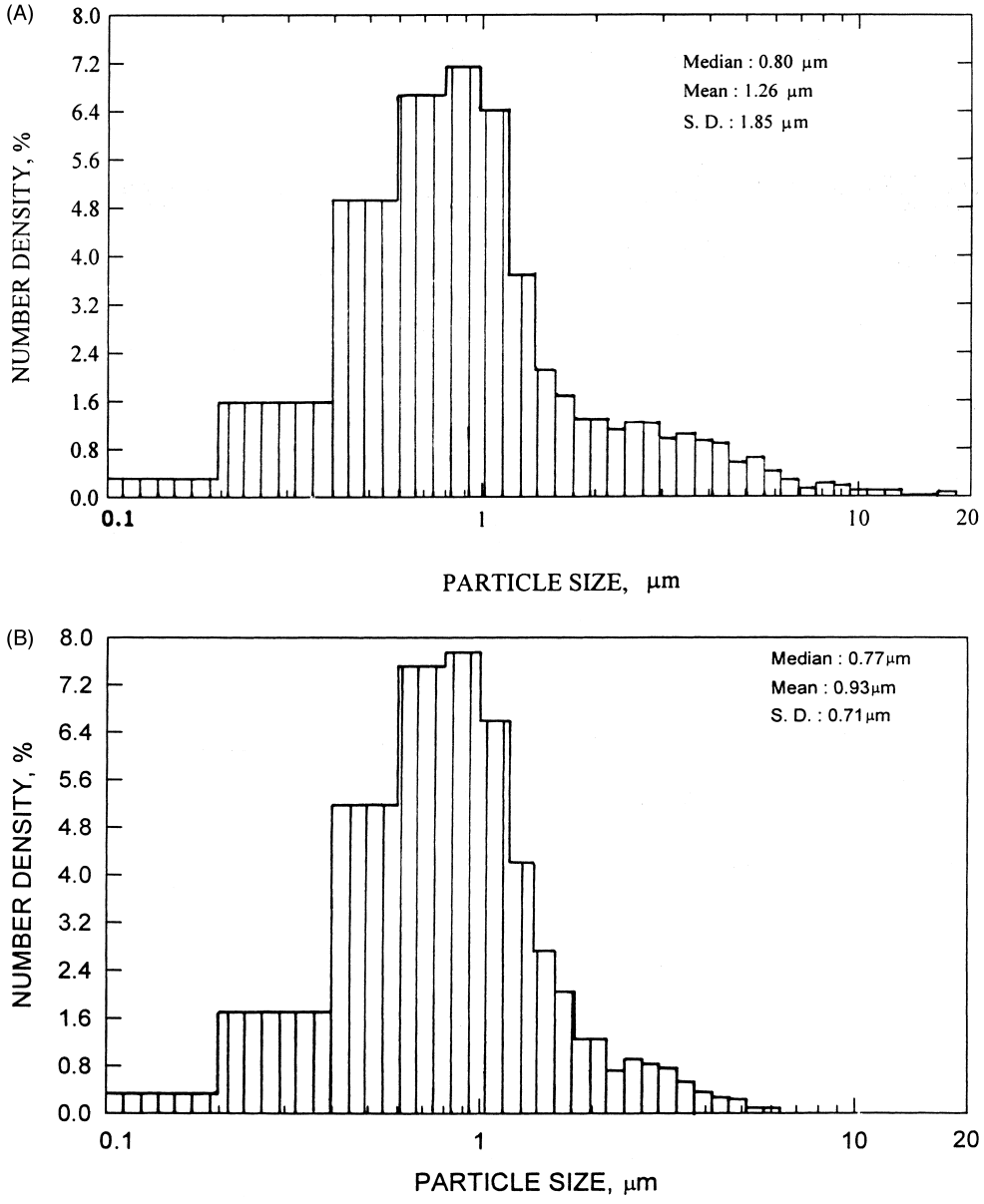

Fig. 5. The particle size distributions of PZT/PLZT precursors calcined at 700°C for 8 h. (A) Powder made from PZT-precursor and (B) powder made from PLZT-precursor.

Livage et al. [22] indicated that the acetate group inhibits the polycondensation process. Since the rates of hydrolysis and polycondensation control the aggregate particle size of the precursor gel, a slower rate of polycondensation should lead to a more monodispersed gel with a smaller aggregate particle size. Indeed the PLZT powder, which contained a larger portion of organic species, exhibited inhibited powder formation compared with the PZT powder. The precursor gel was, as a result, more homogeneous, contained fewer aggregates and had a smaller aggregate particle size.

The calcined PZT and PLZT were analyzed by SEM (Fig. 6). SEM analysis enables the primary particle size of the powders to be determined, as opposed to the particle size distribution given by laser diffraction. The primary particles of the PZT powder were approximately 0.3–0.4 μm in diameter, compared with the PLZT powder particles which were about 0.2–0.3 μm in diameter.

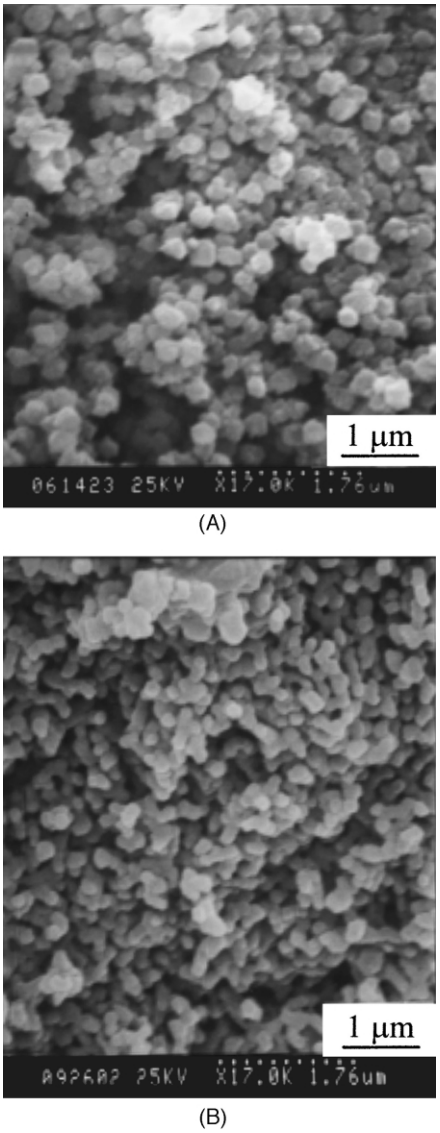

Fig. 6. SEM images of the powders calcined at 700°C. (A) PZT powder, (B) PLZT powder.

The PLZT-gel, due to the fact that $La(OAc)_3$ was added as a starting material, contained a higher mol fraction of acetate groups, which inhibited polycondensation [22]. The slower rate of polycondensation resulted in the product having a smaller particle size [Fig. 6(A)]. DTA/TGA analyses (Fig. 3) suggest that the fraction of chelating acetate groups in the dried precursor is larger for the gel with a high acetic acid ratio. On the other hand, for the gel with a low acetic acid ratio, the percentage of chelating acetate groups is smaller. A chelating acetate group inhibits the polycondensation of the gel. A higher fraction of chelating acetate therefore is directly responsible for a smaller particle size of the ceramic PZT/PLZT powders.

Livage et al. [23] have shown that the isopropoxide group is much more readily hydrolyzed than the acetate group and condensation takes place easily. Evidence from [^{1}H] and [^{13}C] NMR-spectra as well as IR-spectra suggest that if chelating acetate groups are present, the structure around the Ti-ions remains intact, resulting in an inhibition of the condensation process and prolonging the time of gelation. The rates of hydrolysis and polycondensation for the reaction are, therefore, slower and the particle size of the ceramic powder formed is smaller.

3.2.2. Sinterability

After milling for 24 h, PZT and PLZT powders were dried, calcined, compacted in a steel die at 110 MPa and then sintered to obtain bulk ceramics samples of 13 mm in diameter. The sintered samples reached 43–48% of their theoretical density. The theoretical densities of PZT and PLZT are 8.00 and 7.86 g cm^{-1}, respectively [24].

Fig. 7 shows the dilatometric sintering curves of the two ceramics. Dilatometric curves recorded from the disc specimen indicate that sintering took place between 1050 and 1250°C for PZT (with the larger particles, 0.3–0.4 μm in diameter). Measurements of the relative density of the samples (obtained by Archimedes' method) indicate that a relative bulk density maximum for PZT of 94% of theoretical density was reached at a temperature of 1200°C (for 2 h). The relative bulk density of PLZT reached its maximum of 95% of theoretical density at a temperature of 1250°C (for 2 h). The above measurements indicate a relationship between the particle sizes of the powders and their sinterability: the smaller the particles, the more readily the powder sinters. Further sintering experiments revealed that sintering the bulk ceramics at higher temperatures or using longer sintering times can cause the trapping of gas (CO_2 from decarboxylation of still present traces of carbonate) in closed pores, resulting in a decrease of the bulk density. The detected decrease in density could also be due to volatilisation of PbO [25].

3.3. Bulk ceramics properties

3.3.1. Microstructures

The SEM images of the PZT/PLZT specimens that were sintered at various temperatures are shown in Fig. 8. Samples sintered at lower temperatures (1150°C) contained smaller grains but also a considerable amount of pores in their structure, which explains the relatively low density measured for these samples. The grains grew at higher sintering temperatures.

In a normal growth process, the grains grow along the grain boundaries through a grain boundary diffusion process. The driving force causing the growth is interface energy (negative capillary pressure) between the grain boundaries. The interface energy is dependent on the radius of the grain and increases with a decrease in radius, meaning that the driving force for grain-growth is bigger for smaller particles. Smaller particles, in general, sinter more easily than bigger particles. As the sintering process progresses, the grains grow gradually bigger. The grain-growth levels of at a certain grain size though since the grain-growth decreases the overall sinterability of the sample.

Most of the doped La was detected inside the grain itself by SEM mapping (not shown), taking up Pb sites in a solid solution of $(PL,La)(Ti,Zr)O_3$. A small amount also seemed to exist in the grain boundary zone in the form of La_2O_3. The grain boundary zone only has a thickness of 0.1–0.2 μm and is, therefore, relatively small compared to the whole grain (diameter about 5 μm). Since the grain boundary is so thin, it is even possible that the detected amount of La in it is actually an artifact of the La detected inside the grain itself due to the relatively high width of the electron bean used in the detection process. A small amount of La_2O_3 present in the grain boundary zone would give an explanation for the grain-growth inhibition observed in PLZT though. A possible explanation for the inhibited grain-growth and the resulting small particle size is that La_2O_3 has a higher melting point than PLZT and therefore poses a considerable barrier for the diffusion process involved in sintering, assuming that liquid phase sintering is occurring. This would give a further explanation for the fact that, as illustrated in Fig. 8, the PLZT grains are smaller than the PZT grains.

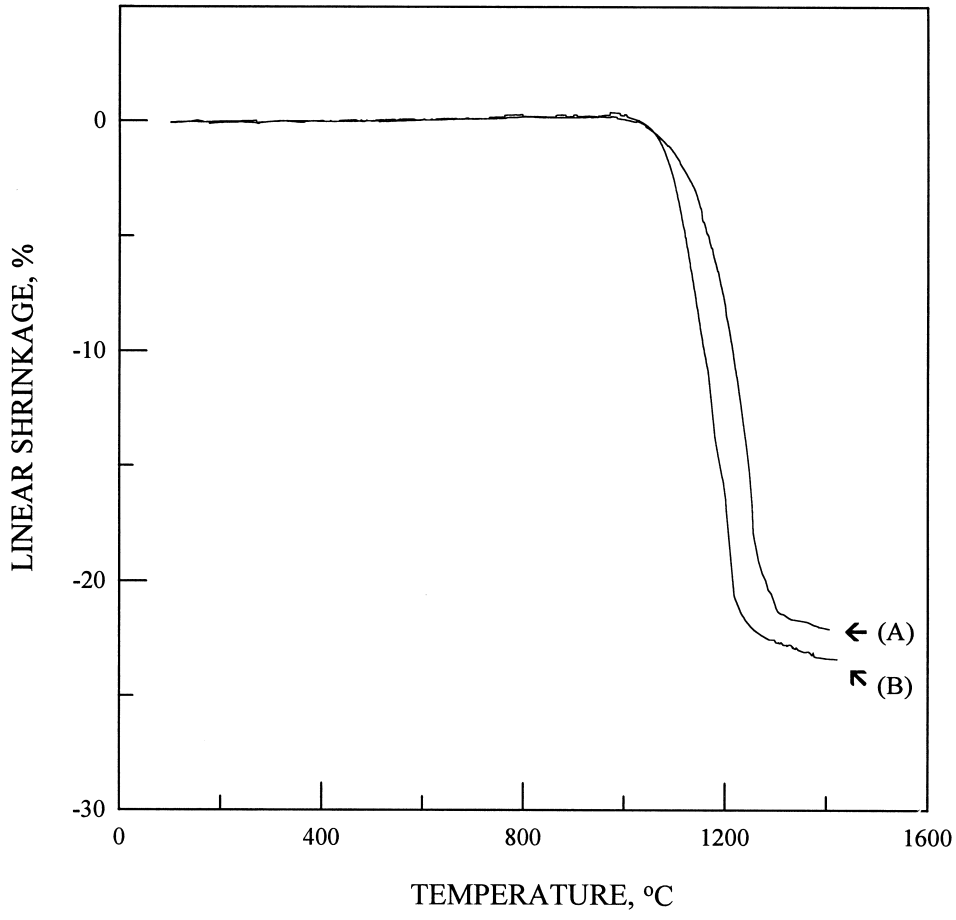

Fig. 7. Dilatometric curves of the compacted PZT and PLZT powders. (A) PZT powder; (B) PLZT powder.

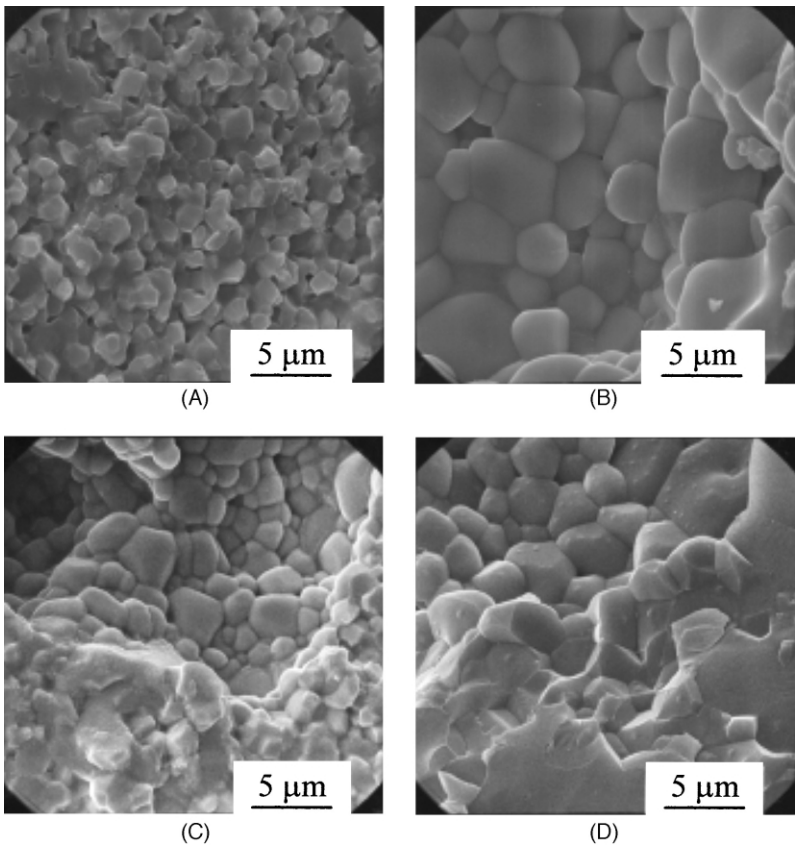

Fig. 8. SEM images of the PZT and PLZT specimens sintered at various temperatures for 2 h. (A) PZT sintered at 1150°C; (B) PZT sintered at 1250°C; (C) PLZT sintered at 1150°C, and (D) PLZT sintered at 1250°C.

3.3.2. XPS surface analysis

The XPS core levels of the PZT bulk ceramics sintered at various temperatures are shown in Fig. 9. Fig. 9(A) shows that the asymmetric Ti 2p peak of the sample sintered at 1150°C, simulated by Gaussians, resolves into three components. The peak at the highest binding energy, centered at 458.9 eV, is attributed to TiO_2 [26,27]. The second peak, centered at 457.8 eV, with a full-width at half maximum (FWHM) of 1.4 eV, is assigned to the Ti^{4+} $2p_{3/2}$ in $Pb(Zr_{0.54},Ti_{0.46})O_3$. The peak position and line splitting are in accordance with the values reported for PZT [28,29]. A third peak is centered at a binding energy of 456.8 eV, with a FWHM of 1.2 eV. The binding energy of the third peak is identified as Ti^{3+} $2p_{3/2}$ in Ti_2O_3 [30–32]. The area ratio of these three peaks is 2: 94: 4, suggesting that the Ti in PZT is the main component in the surface.

Fig. 9(B) shows that the Ti 2p line of the PZT sample sintered at 1200°C also resolves into three peaks. The first one, at 459.6 eV, with a FWHM of 0.8 eV, having a higher binding energy than Ti $2p_{3/2}$ in PZT is attributed to TiO_2. The second one, centered at 457.7 eV, is attributed to Ti in PZT, having a FWHM of 1.5 eV. The third peak, positioned at 456.8 eV, with a FWHM of 1.2 eV, is attributed to Ti_2O_3. According to the peak areas the ratio of TiO_2: PZT: Ti_2O_3 is calculated as 2: 87: 11. The corresponding XPS spectrum of PZT sintered at 1250°C is shown in Fig. 9(C). Ti in TiO_2, PZT and Ti_2O_3 is detected on the surface with a mol ratio of 23: 50: 27.

The XPS core levels of the PLZT bulk ceramics sintered at various temperatures are shown in Fig. 10. Fig. 10(A) shows the sample sintered in air at 1150°C, with binding energies at 458.5, 457.3 and 456.3 eV, which can be assigned to TiO_2, PLZT and Ti_2O_3, respectively. The ratio of TiO_2: PLZT: Ti_2O_3 was calculated as 6: 84: 10. Analysis of the Ti core level energies of the bulk ceramic sintered at 1200°C showed a TiO_2: PLZT: Ti_2O_3 ratio of 8: 74: 18 [Fig. 10(B)]. The ratio for the PLZT sample sintered at 1250°C was 12: 62: 26 [Fig. 10(C)].

Fig. 9 and 10 indicate that a higher sintering temperature results in a higher Ti^{3+} concentration on the surface. An increase of the sintering temperature, therefore, seems to be beneficial to producing surfaces with a relatively high content of lower oxidation state Ti. Comparing PZT and PLZT samples sintered at the same temperature (1100, 1200 and 1250°C), it should also be noted that the Ti^{3+} surface concentration of the PLZT sample is higher than the one in the PZT sample.

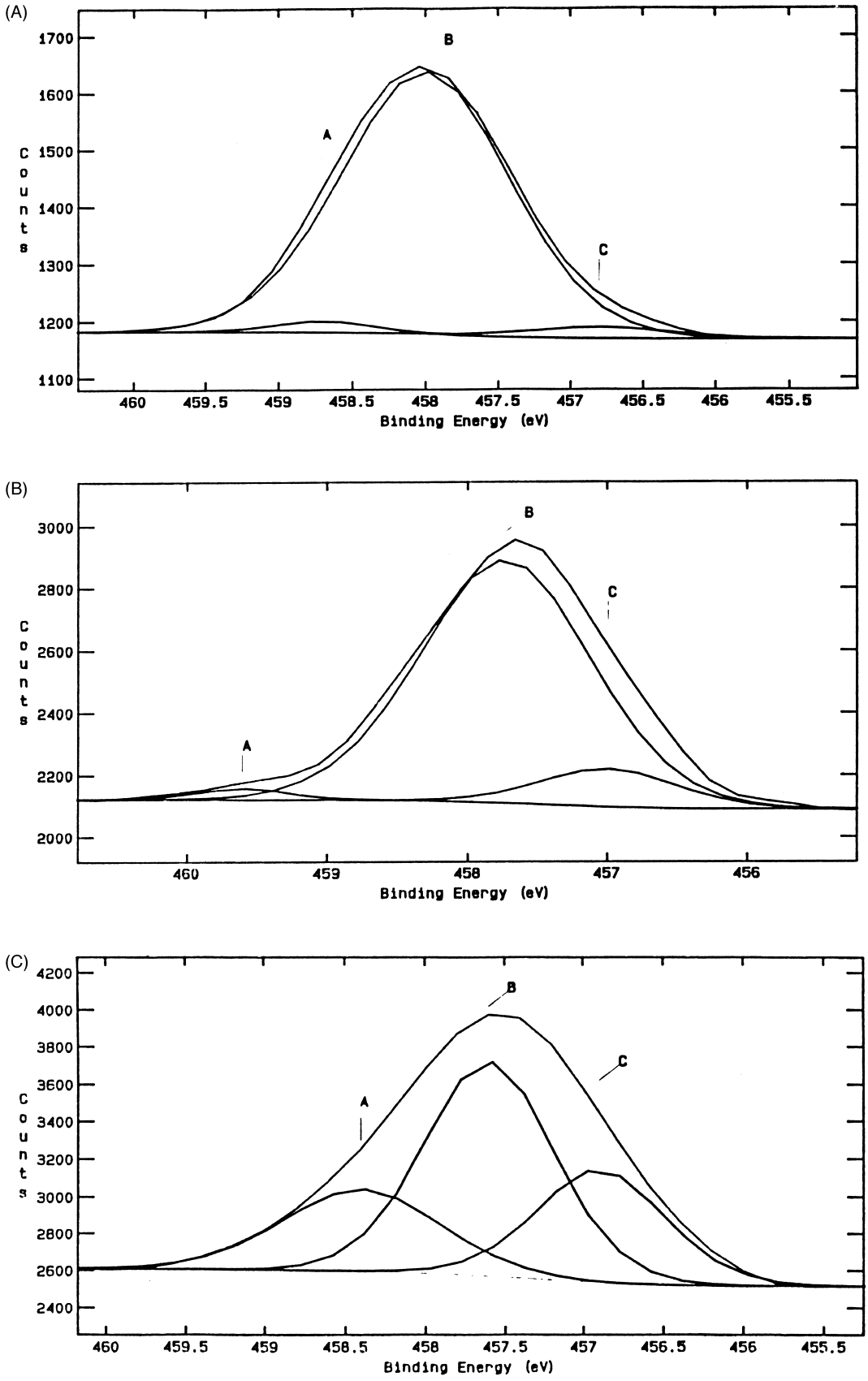

Fig. 9. Ti 2p spectra for the PZT bulks sintered at various temperatures. (A) PZT bulk sintered at 1150°C, (B) PZT bulk sintered at 1200°C; and (C) PZT bulk sintered at 1250°C.

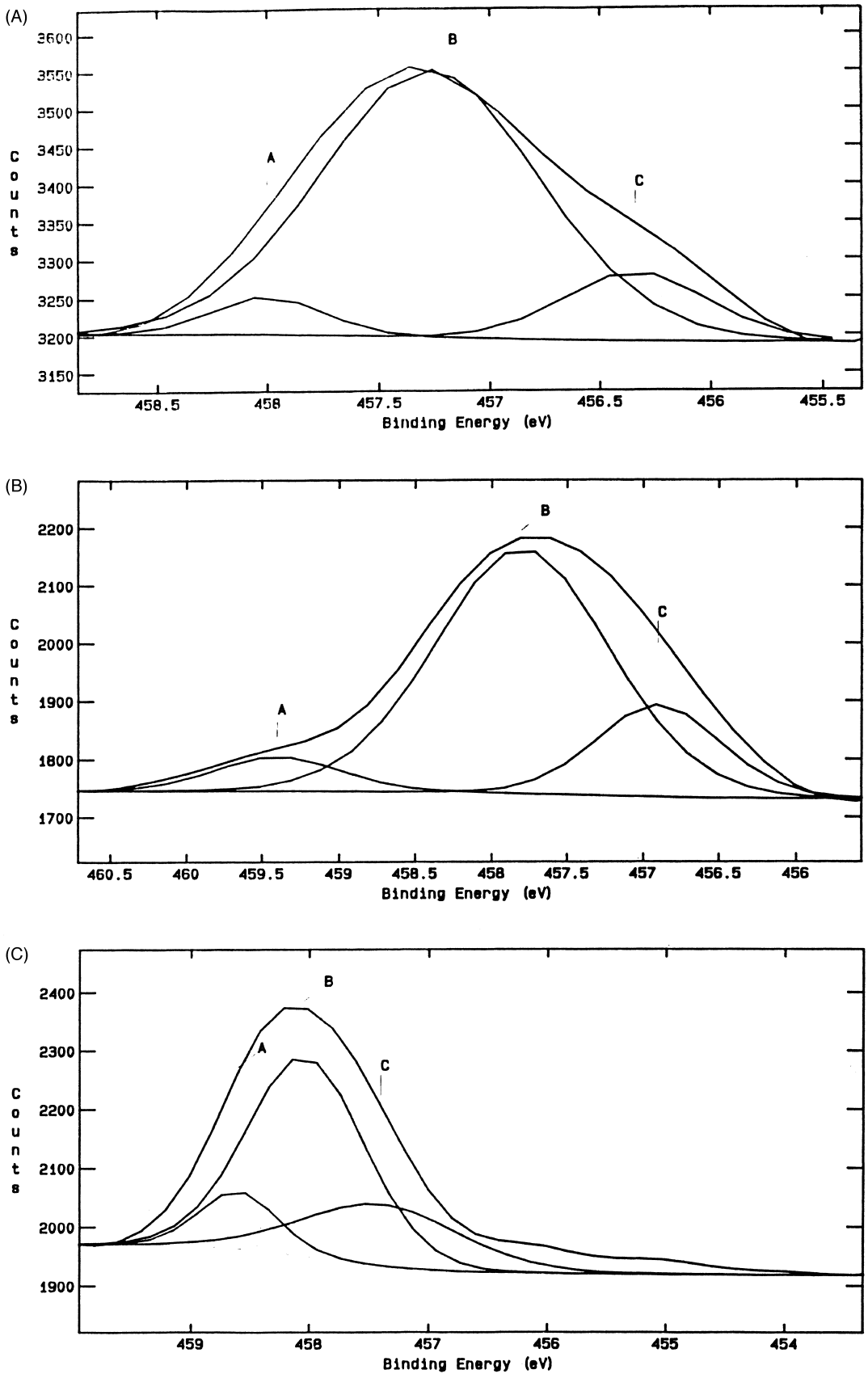

Fig. 10. Ti 2p spectra for PLZT sintered at various temperatures. (A) PLZT sintered at 1150°C, (B) PLZT sintered at 1200°C; and (C) PLZT sintered at 1250°C.

3.3.3. Dielectric properties

The PZT and PLZT powders were compacted and sintered at various temperatures for 2 h. After polishing the surface, their electrical resistivity was measured at 60 Hz. The electrical resistivities of the PZT samples were in the range of 10^7–10^9 Ωcm. For the PLZT samples the range was 10^6–10^8 Ωcm. When PZT and PLZT samples sintered at the same temperature are compared, the PLZT samples always have a lower electrical resistivity than the PZT samples. This correlates with the Ti^{3+} surface concentration. Samples with a higher Ti^{3+} surface concentration in general have a lower electrical resistivity. A Ti^{3+} compound can be described as an electron-rich Ti^{4+} compound (Ti^{4+} e^-). The extra electron can move through the crystal lattice relatively uninhibited and thereby causes the lower electrical resistivity, i.e. better electrical conductivity. As described in the discussion of the XPS results, the PLZT samples sintered at a given temperature all have a higher concentration of surface Ti^{3+}.

The room-temperature relative dielectric constants of the bulk ceramics were measured with a LCR meter (Fig. 11). The relative dielectric constant of PLZT was highest for the sample sintered at a temperature of 1200°C, and then seemed to decrease for samples sintered at higher temperatures to values just outside the margin of error. The measured values for the dielectric constants have an error of ±5%. In contrast, the room-temperature relative dielectric constants of the PZT sample were not significantly affected by the sintering temperature and were always lower than those of the PLZT samples. The relative dielectric constants of the PZT samples were about 550–600, and the relative dielectric constants of the PLZT samples were about 1500, or even higher (up to about 1700) for some sintering temperatures (1150–1200°C).

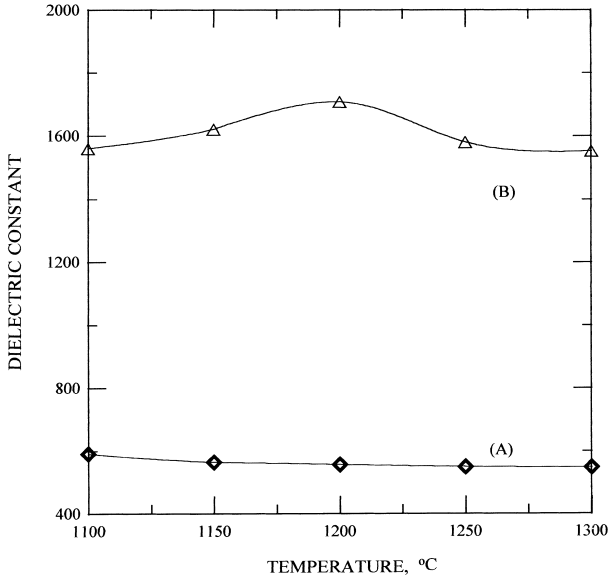

Fig. 11. Relative dielectric constant of the PZT/PLZT sintered at various temperatures.

Combining the XPS study results and the electrical property study results, it can be concluded that at the same sintering temperature more Ti^{3+} existed in the surface of PLZT than PZT. A thin insulative layer of La_2O_3 seemed to exist at the grain boundary. Nevertheless, a low resistivity and a high dielectric constant were observed in the PLZT bulk ceramics. For semiconducting polycrystalline materials in which the grain boundary phase has a high resistivity (here: La_2O_3), the geometrical shape and distribution of the two phases are important [33]. The resulting resistivity and dielectric constant usually vary with frequency, and the low-frequency (here: 60 Hz) dielectric constant can be several orders of magnitude larger than the high-frequency dielectric constant. The presence of the thin insulative La_2O_3 layer does therefore not necessity result in a higher overall resistivity of the material and can be overcompensated by other factors, for example an increased Ti^{3+} concentration.

4. Conclusion

A titanyl zirconyl acetate precursor was obtained by chelating the respective metal alkoxides with acetic acid. This precursor formed a gel through hydrolysis and polycondensation (sol-gel process). After drying and calcination, PZT and PLZT ceramics were obtained.

In this study, high-purity powders of PZT and PLZT were obtained at 700°C. The mechanism of the powder formation was investigated by combining DTA/TGA, FTIR and XRD studies. During the preparation of PZT, the precursor gel decomposed to PbO and TiO_2 which then, in a further step, formed PZT at 600°C. The PLZT-precursor contained a higher mol fraction of acetate groups, which slowed the rate of polycondensation, resulting in a less crosslinked network gel, and the smaller particle size of the PLZT powder.

The PZT and PLZT bulk ceramics were sintered at 1250°C. The room temperature dielectric constant of the PZT bulk ceramics was in the range of 550–600. The dielectric constant of the PLZT samples was about 1500. Measurement of the Ti binding energies on the surface of PZT and PLZT and comparison of the respective XPS peak areas revealed that the total Ti on the PLZT surface contained a higher fraction of Ti^{3+}. A higher concentration of surface Ti^{3+} is responsible for better semiconducting properties, and correlates to the higher dielectric constant of the PLZT ceramic.

Acknowledgements

The author thanks the National Science Council, NSC 88-2214-E-151-003, for the financial support of this work.

References

[1] L. Longtu, Z. Xiaowen, C. Jinghe, Low temperature sintering of PZT ceramics, Ferroelectrics 101 (1990) 101–108.

[2] R.G. Dosch, PZT ceramic from organic-derived precursors, Mater. Res. Soc. Symp. Proc. 32 (1984) 199–211.

[3] B.M Melnick, J.D. Cuchiaro, L.D. Mcmillian, Process optimization and characterization of revise worthy sol-gel based PZT for ferroelectric memories, Ferroelectrics 112 (1990) 329–351.

[4] B. Jaffe, R.S. Roth, S. Marzullo, Properties of piezoelectric ceramics in the solid-solution series, lead titanate–lead zirconate–lead oxide: tin oxide and lead titanate-lead hafnate, J. Res. Nat. Bur. Stand. 55 (1955) 239–254.

[5] R.B. Atkin, R.M. Fulrath, Point defects and sintering of lead zirconate-titanate, J. Am. Ceram. Soc. 54 (1971) 265–271.

[6] K. Okazaki, I. Ohtsubo, K. Toda, Electrical, optical and acoustic properties of plzt ceramics by two stage processing, Ferroelectrics 10 (1976) 195–197.

[7] B.S. Chiou, J.N. Kuo, H.T. Dai, Fabrication and properties of PLZT ceramics from spray-dried aqueous solution, J. Electronic Mater. 20 (1991) 325–330.

[8] P. Duran, C. Moure, High density PLZT ceramics prepared chemically from different raw materials, Am. Ceram. Soc. Bull. 64 (1985) 575–579.

[9] K. Yao, L. Zhang, X. Yao, Controlled crystallization in lead zirconate titanate glass-ceramics prepared by the sol–gel process, J. Am. Ceram. Soc. 81 (1998) 1571–1576.

[10] R. Ostertag, G. Tunker, H. Schmidt, Preparation and properties of sol–gel-derived PZT powders, Brit. Ceram. Proc. 41 (1989) 11–20.

[11] A. Mosset, I. Gautier-Luneau, J. Galy, Sol-gel processed $BaTiO_3$: structural evolution from the gel to the crystalline powder, J. Non-Cryst. Solids 100 (1988) 339–344.

[12] P.P. Phule, S.H. Risbud, Low temperature synthesis and dielectric properties of ceramics derived from amorphous barium titanate gels and crystalline powders, Mater. Sci. Eng. B 3 (1989) 241–247.

[13] C.F. Kao, W.D. Yang, Preparation and electrical properties of fine strontium titanate powder from alkoxide in a strong alkaline solution, Mater. Sci. Eng. B 38 (1996) 127–137.

[14] G.H. Haertling, PLZT thin films prepared from acetate precursors, Ferroelectrics 116 (1991) 51–63.

[15] D. Hennings, G. Rosentein, H. Schreinemacher, Hydrothermal preparation of barium titanate from barium-titanium acetate gel precursors, J. Eur. Ceram. Soc. 8 (1991) 107–115.

[16] G. Phaff, Synthesis of calcium titanate powders by the sol–gel process, Chem. Mater. 6 (1994) 58–62.

[17] R. Ostertag, G. Tunker, H. Schmidt, Preparation and properties of sol–gel-derived PZT powders, Brit. Ceram. Proc. 41 (1989) 11–20.

[18] G. Snow, Fabrication of transparent electro-optic PLZT ceramics by atmosphere sintering, J. Am. Ceram. Soc. 56 (1973) 91–96.

[19] C. Sancher, J. Livage, M. Henry, F. Babonneau, Chemical modification of alkoxide precursors, J. Non-Cryst. Solids 100 (1988) 65–76.

[20] P.P. Phule, S.H. Risbud, Sol-Gel synthesis of barium titanate powders using barium acetate and titanium isopropoxide, Adv. Ceram. Mater. 3 (1988) 183–185.

[21] B. Samuneva, D. Jambazov, D. Lepkova, Y. Dimitriev, Sol–gel synthesis of $BaTiO_3$ and $Ba_{1-x-y}Ca_ySr_x(Zr_yTi_{1-y})O_3$ perovskite powders, Ceram. Int. 16 (1990) 355–360.

[22] J. Livage, C. Sanchez, M. Henry, S. Doeuff, The chemistry of the sol–gel process, Solid State Chem. 32/33 (1989) 633–638.

[23] S. Doeuff, M. Henry, C. Sanchez, J. Livage, Hydrolysis of titanium alkoxides: modification of the molecular precursor by acetic acid, J. Non-Cryst. Solids 89 (1987) 206–216.

[24] N.D. Patel, P.S. Nicholson, Composition of piezoelectric properties of hot-pressed and sintered PZT, Am. Ceram. Bull. 65 (1986) 783–787.

[25] R. Ostertag, G. Tunker, H. Schmidt, Preparation and properties of sol–gel-derived PZT powders, Brit. Ceram. Proc. 41 (1989) 11–20.

[26] G. Rocker, W. Gopel, Titanium overlayers on TiO_2 (100), Surface Sci. 18 (1987) 530–558.

[27] V.E. Henrich, The surfaces of metal oxides, Rep. Prog. Phys. 48 (1985) 1481–1541.

[28] H. Ikawa, T. Yamada, X-ray photoelectron spectroscopy study of high- and low-temperature forms of zirconium titanate, J. Am. Ceram. Soc. 74 (1991) 1459–1462.

[29] C.D. Wagner, W.M. Riggs, L.E. Davis, J.F. Moulder, G.E. Miulenberg, Handbook of X-ray photoelectron spectroscopy, Perkin-Elmer, Eden Prairie, MN, 1979, p. 68.

[30] N.R. Armstrong, R.K. Quinn, Auger and X-ray photoelectron spectroscopic and electrochemical characterization of titanium thin flim electrodes, Surface Sci. 67 (1977) 451–468.

[31] A.F. Carley, P.R. Chalker, J.C. Riviere, M.W. Roberts, The identification and characterisation of mixed oxidation states at oxidised titanium surfaces by analysis of X-ray photoelectron spectra, J. Chem. Soc., Faraday Trans. 1 83 (1987) 351.

[32] M.E. Levin, M. Salmeron, A.T. Bell, G.A. Somorjai, The characterization of Ti and Al oxide overlayers on rhodium and gold by XPS, Surface Sci. 195 (1988) 429–442.

[33] W.D. Kingery, H.K. Bowen, D.R. Uhlmann. Introduction to ceramics, 2nd Edition, John Wiley & Sons, New York 1976, pp. 947–951.